Ecological Modelling 246 (2012) 91–98

Contents lists available at SciVerse ScienceDirect

Ecological Modelling

journal homepage: www.elsevier.com/locate/ecolmodel

Influences of diurnal rainfall cycle on CO_2 exchange over Bornean tropical rainforests

Tomo'omi Kumagai[a,*], Tomonori Kume[b]

[a] Hydrospheric Atmospheric Research Center, Nagoya University, Chikusa-ku, Nagoya 464-8601, Japan
[b] School of Forestry and Resource Conservation, National Taiwan University, Taipei 106, Taiwan

ARTICLE INFO

Article history:
Received 29 March 2012
Received in revised form 30 June 2012
Accepted 9 July 2012

Keywords:
Southeast Asia
CO_2 flux
Photosynthesis
Precipitation
Multilayer model

ABSTRACT

In the Southeast Asian tropics, distinct peaks of the diurnal precipitation cycle at specific times of the day are among the dominant features of environmental factors. Although the characteristics of rainfall timing during the day are anticipated to affect the ecosystem CO_2 flux (N_E), no attempt has been made to quantify the impact. To address this issue, the potential alteration of N_E corresponding to a change in the diurnal rainfall regime was investigated using a combination of detailed field measurements conducted at an eddy flux observation site, computation with a multilayer soil–vegetation–atmosphere transfer model, and rainfall time series constructed from rainfall statistics of observation-site data and published data of long-term diurnal precipitation cycles over Borneo. The results showed that there was little difference in the mean diurnal N_E pattern between "wet" and "dry" days (days with and without rainfall, respectively) and the diurnal rainfall regime little affected N_E on a whole-year scale. Similar N_E values for wet and dry days might be attributed to (1) a minor contribution of lower N_E during rainfall events to total N_E in wet conditions, because of constant cloud cover on both wet and dry days and (2) the light saturation of N_E at relatively low incident radiative energy (≈500 W m^{-2} of solar radiation) in this forest ecosystem.

1. Introduction

Southeast Asian tropical rainforests are among the most important biomes in terms of annual productivity and water cycling; hence, small perturbations in such biomes could result in a significant change in the global carbon cycle (e.g., Taylor and Lloyd, 1992). The projected growth in atmospheric greenhouse gases within the coming century will significantly affect global and regional temperatures with concomitant changes in precipitation patterns, and deforestation and land use change in tropical forests could also lead to global and regional precipitation changes (e.g., Nobre et al., 1991; Mabuchi et al., 2005; Werth and Avissar, 2005). An analysis of climatic trends of global tropical rainforest regions showed that rainfall appears to have declined more significantly in Southeast Asia (SEA) than in Amazonia, and that the El Niño Southern Oscillation (ENSO) is the primary driver inducing drought in SEA (Malhi and Wright, 2004). Note that results from a global climate model showed more frequent El Niño-like conditions due to human-induced greenhouse warming (Timmermann et al., 1999). Kumagai et al. (2009) examined the impact of both intra (seasonal) and interannual (ENSO-related) variations in precipitation on hydrologic fluxes in a SEA tropical rainforest.

Characteristics of diurnal precipitation cycles in the SEA region have been also investigated, and it was found that there are distinct peaks of the diurnal precipitation cycle at specific times of the day for each location in the SEA tropics (e.g., Oki and Musiake, 1994; Ohsawa et al., 2001; Ichikawa and Yasunari, 2006). According to analyses using 3-year Tropical Rainfall Measuring Mission (TRMM) satellite measurements (Nesbitt and Zipser, 2003), the diurnal precipitation cycle over the ocean has low amplitude. The maximum contribution to rainfall is in the early morning, because of an increased number of mesoscale convective systems in the nighttime. Also, land areas have a much larger precipitation cycle than those over oceans, with a maximum in the afternoon caused by enhancement by afternoon heating. Ohsawa et al. (2001) suggested that diurnal precipitation cycles in the SEA region are generated by interaction between local circulation influenced by topographic effects and an upper-level flow component. Thus, the cycles are anticipated to change according to variations of atmospheric convective activity on local and global scales. Since exchanges between forest canopy and atmosphere such as assimilation and evapotranspiration are driven mainly by solar radiation, their activities might be influenced by the precipitation timing during the day via the effects of weak incident solar radiation, low vapor-pressure deficit

* Corresponding author at: Hydrospheric Atmospheric Research Center, Nagoya University, F3-1 (200) Furo-cho, Chikusa-ku, Nagoya, Aichi 464-8601, Japan. Tel.: +81 52 789 3478; fax: +81 52 789 3436.
E-mail address: tomoomikumagai@gmail.com (T. Kumagai).

0304-3800/$ – see front matter © 2012 Elsevier B.V. All rights reserved.
http://dx.doi.org/10.1016/j.ecolmodel.2012.07.014

and leaf wetness (see Tanaka, 2002; Kume et al., 2006). In addition, rainfall pulses, especially in arid and semi-arid ecosystems, affect soil respiration and hence ecosystem CO_2 flux (N_E; $\mu mol\ m^{-2}\ s^{-1}$) (e.g., Huxman et al., 2004), and Knapp et al. (2002) suggested that soil respiration is dependent not only on the precipitation amount but also on the frequency of rainfall occurrence. There seems to be mixed evidence for this pulsation effect in moist environments (e.g., Palmroth et al., 2005; Daly et al., 2008). Thus, the change in the diurnal precipitation cycle might alter energy and carbon exchanges between SEA tropical forest canopy and atmosphere. To our knowledge, no study has considered the potential alteration of the canopy exchanges due to changes in the diurnal precipitation pattern.

The primary objective of this study, therefore, is to understand how N_E of a lowland dipterocarp forest in the SEA humid tropics responds to the diurnal rainfall regime. The rainfall regime affects incident solar radiation and atmospheric humidity; increases of radiation and vapor pressure deficit, respectively, directly increase N_E, and indirectly decrease it through a reduction of stomatal conductance. Thus, a concrete goal is to show the impact of interplay between solar radiation and atmospheric humidity on N_E during rainfall events. Toward this objective, we used a combination of detailed field measurements recorded at an eddy flux observation site (Kumagai et al., 2004a,b; Manfroi et al., 2006; Ohashi et al., 2008) and a multilayer soil–vegetation–atmosphere transfer (SVAT) model (Kumagai et al., 2006). For further investigation of potential changes in N_E caused by alteration of the diurnal rainfall regime, N_E was computed by the SVAT model with input of a 30-min interval rainfall time series constructed using the rainfall statistics of the observation site data and published data of long-term diurnal precipitation cycles over Borneo (see Oki and Musiake, 1994).

2. Study sites

Vegetation–atmosphere exchange and meteorological data, well suited for estimating the SVAT model parameters, were obtained for a natural forest in Lambir Hills National Park (LHNP; 4°12′N, 114°02′E, 200 m a.s.l.) 30 km south of Miri City, Sarawak, Malaysia (Fig. 1A). The rainforest in LHNP consists of two types of original vegetation common to Borneo, mixed dipterocarp and tropical heath forest. The former contains various genera of the family Dipterocarpaceae, which covers 85% of LHNP. The average canopy height in the study site is about 40 m but the heights of the emergent treetops can reach 50 m. Spatial variations in leaf area plus branches (plant area index; PAI) were measured using a pair of plant canopy analyzers (Kumagai et al., 2006). In this study, leaf area index (LAI) is assumed to be PAI. The LAI ranged spatially from 4.8 to 6.8 $m^2\ m^{-2}$ with a mean of 6.2 $m^2\ m^{-2}$. The monthly amounts of litterfall were similar throughout the year, perhaps suggesting small variations in the LAI.

An 80 m tall (at the base of a gondola) canopy crane with a 75 m long rotating jib and gondola was used for measurements of the spatial variations in leaf-level physiological parameters and leaf area density, eddy-covariance flux measurements, and above-canopy meteorological measurements. In a subplot about 70 m from the crane, measurements of the in-canopy microclimate and CO_2 concentration profile and soil environment such as measurements of soil moisture, soil heat flux and soil respiration were carried out. Time series of the wind speed and gas concentration were sampled at 10 Hz using a three-dimensional sonic anemometer co-located with an open-path CO_2/H_2O analyzer. All variances and covariances required for eddy-covariance flux estimates were computed over a 30-min averaging interval. Air samples were obtained at six heights using pumps and an auto switching system, and CO_2 concentrations were measured using a closed-path CO_2 analyzer. N_E was derived as the sum of the above-canopy CO_2 flux, which was obtained using the eddy covariance system above the canopy, and the within-canopy storage flux, which was determined by quantifying the rate of change of CO_2 concentration in the air column within the canopy. Comparison between the daily accumulation of the above-canopy CO_2 flux and N_E confirmed the possibility of ignoring the drainage flow effects at this site. Available data of the above-canopy CO_2 flux covered 41% of the period between 1 June 2001 and 29 October 2002. Further details of the experimental setup and data processing are presented elsewhere (Kumagai et al., 2004a,b; Manfroi et al., 2006; Ohashi et al., 2008).

The temperature in LHNP has an annual mean of around 27 °C and little seasonal variation. The mean annual rainfall in LHNP for the period 2000–2006 was around 2600 mm, while that at Miri Airport, 20 km from LHNP, for the period 1968–2001 was around 2740 mm. Annual rainfall cycles in LHNP and at Miri Airport were similar; although there was scarce seasonality, the drier and wetter months were between February and September and between October and January, respectively, at both locations. A distinct diurnal rainfall cycle was characteristic of LHNP; typically, there were intense storms in the afternoon (around 1200–1600 LT) and midnight (around 2200–0200 LT), and durations of the rainfall events in the afternoon and midnight were about 1 and 4.5 h, respectively (Fig. 1B and C).

For reproducing the diurnal rainfall cycle regime and computing potential change in N_E corresponding to regime, 10-year data of two other characteristic diurnal precipitation cycles from Bintulu (3°12′N, 113°00′E, 3 m a.s.l.) and Kuching (1°30′N, 110°18′E, 30 m a.s.l.), about 100 and 450 km southwest of Miri, respectively, were used to obtain diurnal rainfall statistics (Fig. 1A) (see Oki and Musiake, 1994). Seasonal rainfall cycles at both sites were similar to that in LHNP, and the mean annual rainfall for the period 1981–1990 in Bintulu and Kuching was 3687 and 3981 mm, respectively. The diurnal rainfall cycles in Bintulu and Kuching contrasted with that in LHNP, and had a strong peak of precipitation at midnight (around 2200–0500 LT) and in the afternoon (around 1500–1800 LT), respectively (Fig. 1A). It is interesting to note that in western coastal areas of Borneo, a diurnal rainfall pattern at a given site corresponds to the distance between the site and the coast; the site nearest the coast (e.g., Bintulu) and the inland site (e.g., Kuching) have midnight and afternoon precipitation peaks, respectively, and the location of LHNP is somewhat between Bintulu and Kuching in terms of the distance from the coast.

3. Theory

3.1. SVAT model description

The simulations were conducted with a one-dimensional multilayer SVAT model, configured with 1500 and 50 layers for computing turbulent statistics and scalar source/sink distributions, respectively (Kumagai et al., 2006). The SVAT model consists of three submodels: (1) a model for energy and radiation conservation, (2) an ecophysiological model for stomatal opening and carbon assimilation, and (3) a model for turbulent diffusion. In the present model, the soil respiration (R_{soil}) model was revised using long-term R_{soil} data (Ohashi et al., 2008) so that R_{soil} can be properly simulated on a longer time scale. Note that the model used here was parameterized with independently collected ecophysiological measurements and was not calibrated or parameterized with canopy-level flux measurements. Although a previous study, Kumagai et al. (2006), provided detailed information, brief review and description of this modeling scheme are presented below for completeness.

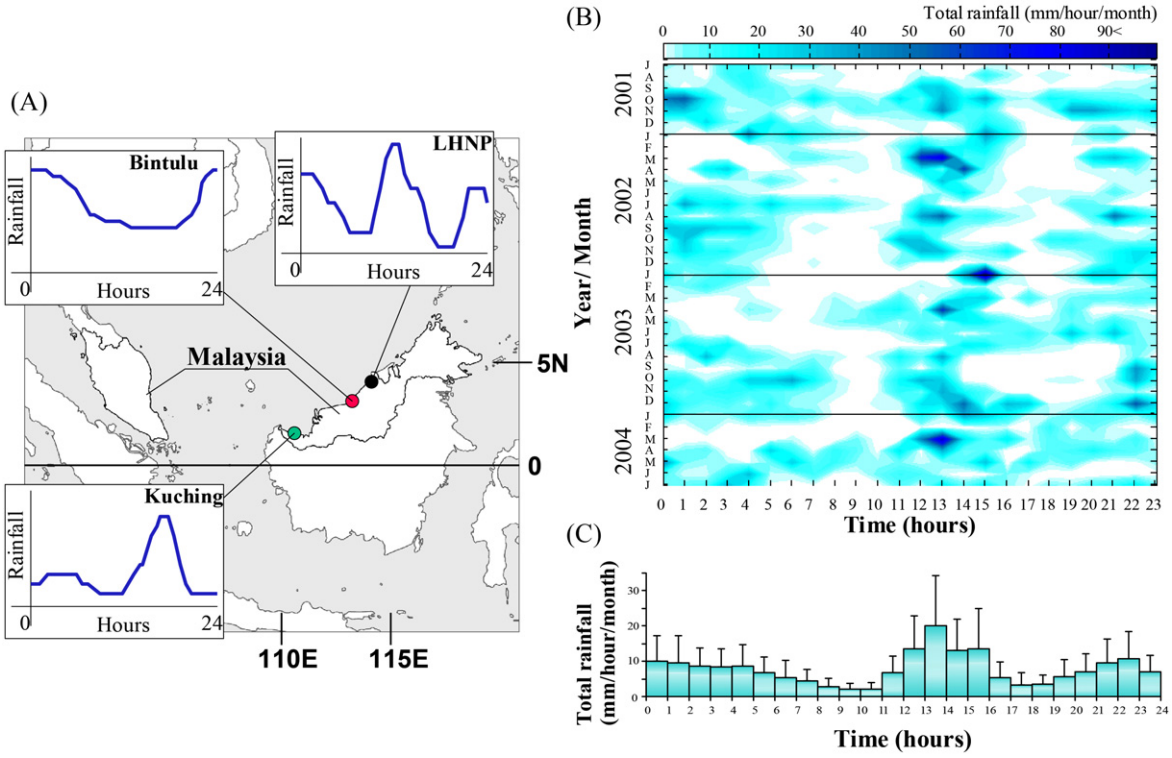

Fig. 1. (A) Locations of LHNP (Lambir Hills National Park), Bintulu and Kuching and a schematic representation of the diurnal precipitation cycle at each study site. (B) Rainfall intensity at various times of a day in each month, and (C) hourly average rainfall intensity over the study period, with vertical bars representing +1 standard deviation in LHNP.

Redrawn from Manfroi et al. (2006).

3.1.1. Radiative transfer and energy balance at both leaf and soil surface levels

When considering the leaf-scale energy balance together with photosynthesis within a forest canopy, the radiative transfer through the canopy must be determined. Then, direct beam and diffuse irradiance must be considered separately due to their different attenuations in the canopy. The probability of no contact within a canopy layer for beam irradiance (P_b) needs to be formulated for describing the direct irradiance transfer within the canopy. This formulation includes the leaf area density (a_{leaf}), the beam extinction function of solar elevation and leaf angle distribution within a given layer (see Goudriaan, 1977). The probability of no contact within a canopy layer for diffuse irradiance (P_d) is calculated by integrating P_b over the solid angles of the sky hemisphere.

Both direct and diffuse solar radiation can be further divided into photosynthetic active radiation (PAR) and near-infrared radiation (NIR) according to their different absorption by leaves. Fortunately, approximately half the global solar radiation (R_s) over the canopy is in the form of PAR while the other half is in the form of NIR, enabling estimates of R_s penetration inside the canopy. The absorbed PAR or NIR within a canopy layer between z (the height from the ground) and $z + \Delta z$, ΔS, is defined as:

$$\Delta S_b = (1 - \eta - \xi)(1 - P_b)S_b(z + \Delta z) \quad (1)$$

$$\Delta S_d^{\downarrow} = (1 - \eta - \xi)(1 - P_d)S_d^{\downarrow}(z + \Delta z) \quad (2)$$

$$\Delta S_d^{\uparrow} = (1 - \eta - \xi)(1 - P_d)S_d^{\uparrow}(z) \quad (3)$$

where η and ξ are the leaf transmissivity and reflectivity, respectively, for PAR or NIR, and S is PAR or NIR at the given height. The subscripts b and d denote direct beam and diffuse irradiation, respectively, and superscript arrows denote the direction of the irradiation. Because P_b and P_d are complex functions of the leaf area density, leaf angle distribution and foliage clumping factor within a given canopy layer and the solar geometric direction (see Kumagai et al., 2006), Eqs. (1)–(3) are not readily solved. The total absorbed solar radiation within the canopy layer is then calculated as the sum of the absorbed PAR and NIR, both of which are calculated by Eqs. (1)–(3). Sunlit leaves receive the beam and the upward and downward diffuse radiation, while shaded leaves only receive upward and downward diffuse radiation. Therefore, the irradiance absorption and energy balance need to be computed separately for sunlit and shaded leaves (see Kumagai et al., 2006).

Assuming that soil heat storage can be neglected (see Kumagai et al., 2006), the energy balance at the soil surface for computing T_{soil}, is expressed by:

$$R_{sab\_soil} + R_{L\_down}(0) - \varepsilon_s\sigma(T_{soil} + 273)^4 = LE_{soil} + H_{soil} \quad (4)$$

where R_{sab_soil} is the total R_s absorbed by the soil surface, R_{L_down} (0) is downward long-wave radiation (R_L) at $z = 0$, ε_s is the soil emissivity, σ is the Stefan–Boltzmann constant (5.67×10^{-8} W m^{-2} K^{-4}), and LE_{soil} and H_{soil} are latent and sensible heat fluxes at the soil surface, respectively. LE_{soil} and H_{soil} are the functions of T_{soil}, as described by the products of the transport conductance and the concentration difference. In addition, the soil surface moisture availability was also used for the LE_{soil} computation (see Kumagai et al., 2006).

3.1.2. Leaf-level physiological functions

The leaf-level scalar source strengths, i.e., leaf sensible heat (H_l: W m^{-2}), transpiration (E_l: kg m^{-2} s^{-1}) and photosynthesis rate (A_l: μmol m^{-2} s^{-1}) are derived from physiological controls using:

$$H_l = 2m_a c_p g_{ah}(T_l - T_a) \quad (5)$$

$$E_l = m_e \frac{g_{aw}g_{sw}}{g_{aw} + g_{sw}} \frac{[e_{sat}(T_l) - e]}{p_a} \quad (6)$$

$$A_l = g_{ac}(C_a - C_s) \quad (7)$$

$$A_l = g_{sc}(C_s - C_i) \quad (8)$$

where m_a and m_e are the molecular weights of air and water (kg mol^{-1}), respectively, $e_{sat}(T_l)$ and e are the saturation vapor pressure at leaf temperature (T_l) and atmospheric water vapor pressure (Pa), respectively, p_a is the atmospheric pressure (Pa), and C_s, C_a and C_i are the CO_2 concentrations (μmol mol^{-1}) of air inside and outside the laminar boundary layer of leaves and within the stomatal cavity, respectively. g_{ah}, g_{aw} and g_{ac} are the boundary layer conductances for heat, water vapor and CO_2 (mol m^{-2} s^{-1}), respectively, calculated according to Campbell and Norman (1998).

g_{sw} and g_{sc} are the stomatal conductances for water vapor and CO_2 (mol m^{-2} s^{-1}), respectively. g_{sc} is linked to A_l, the relative humidity of air inside the boundary layer of a leaf (h_s) and C_s, as described by Ball et al. (1987) and Collatz et al. (1991), and is given by:

$$g_{sc} = m_L \frac{A_l h_s}{C_s} + b_L \quad (9)$$

where m_L and b_L are the slope and intercept, respectively, and were obtained by linear regression analysis of data from leaf-level gas exchange measurements. g_{sw} is obtained from $g_{sw} = 1.6\, g_{sc}$, where 1.6 is the ratio of diffusivities of water and CO_2 in air (von Caemmerer and Farquhar, 1981).

A_l was computed using the biochemical model of Farquhar et al. (1980) and Collatz et al. (1991) as a minimum value of the gross rate of photosynthesis limited by the rate of RuBP regeneration through electron transport (J_E), RuBP carboxylase–oxygenase (Rubisco) activity (J_C) and the export rate of synthesized sucrose (J_S), as:

$$A_l = \min\{J_E, J_C, J_S\} - R_d \quad (10)$$

where R_d is the respiration rate during the day but in the absence of photorespiration. The formulation and parameterization of J_E, J_C, J_S and R_d as a function of PAR absorbed by the leaf, CO_2 concentration within the stomatal cavity and leaf temperature is used from Farquhar et al. (1980), Farquhar and Wong (1984), Collatz et al. (1991) and de Pury and Farquhar (1997). The photosynthesis model constants can be determined according to Badger and Collatz (1977), Farquhar et al. (1980), von Caemmerer et al. (1994) and de Pury and Farquhar (1997). The V_{cmax} and the J_{max} used in these calculations are expressed as non-linear functions of temperature using values at 25 °C (V_{cmax_25} and J_{max_25}, respectively); the formulations of which are given in de Pury and Farquhar (1997). In addition, R_d is expressed as a non-linear function of temperature using R_d at 25 °C (R_{d_25}), which was assumed to be linearly related to V_{cmax_25} (as in Collatz et al., 1991). Practically, both J_{max_25} and R_{d_25} are related to V_{cmax_25}, and hence, V_{cmax_25} is the key parameter in the leaf photosynthesis model.

3.1.3. Scalar transport

The scalar continuity and turbulent flux equations are obtained by assuming a steady state planar-homogeneous and high Reynolds and Peclet numbers flow, and by applying time and horizontal averaging (see Katul and Albertson, 1999). In the scalar continuity equations, the source (or sink) terms, due to mass release (or uptake) by the ensemble of leaves within the averaging plane, are given by:

$$S_T = \frac{1}{\rho_a c_p}(H_{lsl} a_{sl} + H_{lsh} a_{sh}) \quad (11)$$

$$S_q = \frac{1}{\rho_a}(E_{lsl} a_{sl} + E_{lsh} a_{sh}) \quad (12)$$

$$S_c = -(A_{lsl} a_{sl} + A_{lsh} a_{sh}) \quad (13)$$

where S_T, S_q and S_c are the source strengths for heat (K s^{-1}), water vapor (kg kg^{-1} s^{-1}) and the CO_2 concentration (μmol m^{-3} s^{-1}), respectively, ρ_a is the density of air (kg m^{-3}), c_p is the specific heat of air at constant pressure (J kg^{-1} K^{-1}), and a denotes a_{leaf}. Subscripts sl and sh denote sunlit and shaded leaves, respectively. The turbulent flux equations include unknowns requiring closure approximations for flux transport and pressure scalar gradient covariance as described by Mellor (1973).

To solve the scalar continuity and turbulent flux equations, velocity statistics within the canopy need to be computed. Here, the second-order closure model formulated by Wilson and Shaw (1977) was applied. Using the measured wind profile and logarithmic law, the momentum roughness length and zero-plane displacement were determined as 0.047h and 0.89h respectively (where h is the canopy height). Note that these values were used to adjust the wind speed measured at the top of the tower to the actual friction velocity. Boundary conditions were specified in accordance with Katul and Albertson (1999), and the closure constants given by Wilson and Shaw (1977), Watanabe (1993) and Katul and Albertson (1999) were used. To solve the second-order closure model, we used the numerical scheme as described by Katul and Albertson (1998, 1999).

3.2. Generation of time series of environmental factors

To compute N_E in LHNP, Bintulu, and Kuching, time series of environmental factors for the sites, which are driving forces for the SVAT model, were constructed using random numbers generated from probability distributions. The rainfall time series was a primary driver generating the other factor time series, and their generation is described as follows.

The inter-arrival times of rainfall events were assumed to be a stochastic variable extracted from an exponential distribution, in which the mean interval time (in days) was derived for each site from long-term precipitation records (see Oki and Musiake, 1994; Kumagai et al., 2009). Here we defined "wet" and "dry" days, which refer to days with and without rainfall events, respectively. As a result, annual mean wet and dry days were respectively estimated to be 196 and 169 days for Miri, 227 and 138 days for Bintulu, and 235 and 130 days for Kuching.

Using data of the annual mean wet days and the total rainfall observed in a given hour of a day over the study period such as those in Fig. 1C, the mean depths for each hour (i) on a given wet day (α_i: mm 30 min^{-1}) were estimated for each site. Rainfall intensity for each hour on a wet day (h_i: mm 30 min^{-1}) was assumed to be an independent random variable expressed by a Poisson process with the parameter α_i. Although the rainfall data interval was hourly, the unit of the generated rainfall intensity variable was converted to per 30 min, to be consistent with data of eddy flux and meteorological factors. Note that this assumption can be validated by the observation that the standard deviation of h_i was approximately equal to its mean value; i.e., α_i (see Fig. 1C) (e.g., Taylor and Karlin, 1998).

The time series of other above-canopy meteorological factors such as incident solar radiation (R_s; W m^{-2}), long-wave radiation (R_L; W m^{-2}), wind speed (U; m s^{-1}), air temperature (T_a; °C) and specific humidity (q_a; kg kg^{-1}) were obtained as follows: On a dry day, R_s in a given hour (i) of the day was generated as a random number from the Gaussian representing the distribution of R_s in each hour (Fig. 2). However, on a wet day, first the ratio of R_s on wet days to that on dry days was generated from its Gaussian distribution in each bin range of rainfall intensity, which is determined by the generated h_i. Then R_s on a wet day was computed from products of the generated ratio and R_s generated in a given hour on a dry day (Fig. 2). Finally, R_L, U, T_a and q_a values related to R_s for both

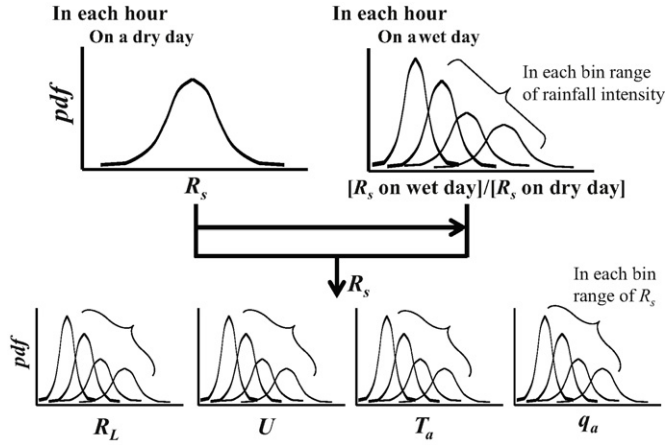

Fig. 2. Schematic diagram of process to obtain above-canopy meteorological factors, incident solar radiation (R_s), long-wave radiation (R_L), wind speed (U), air temperature (T_a) and specific humidity (q_a), using random number generation from each probability density function (*pdf*).

a dry and a wet day were obtained as random numbers, generated by a Gaussian representing the distribution of each meteorological factor in each bin range of R_s (Fig. 2). We confirmed that, using this technique, all environmental factors were reproduced well in terms of their means and standard deviations.

4. Results and discussion

4.1. Analyses for LHNP

For practical implementation of the SVAT model in this analysis, it is first necessary to examine how sensitive the flux calculations are to micrometeorological factors during a rainfall event. Examples of comparisons between modeled and measured N_E in LHNP are shown under four typical meteorological conditions; i.e., a rainfall event at noon (Fig. 3a and e), rainfall event from midnight to early morning and cloud during daylight hours (Fig. 3b and f), cloudy with little rainfall (Fig. 3c and g), and midnight rainfall and clear sky during daylight hours (Fig. 3d and h). It should be noted that there were two types of abrupt declines of N_E and solar radiation (R_s) at noon on 6 September with rainfall (Fig. 3a and e) and 11 September without rainfall (Fig. 3c and g). Note that the model accurately reproduced measured N_E for the entire available data period including periods of the four abovementioned meteorological conditions; regression statistics for comparisons between the measured and modeled values had a slope of 0.79, intercept of $-0.80\ \mu mol\ m^{-2}\ s^{-1}$, R^2 of 0.62 and a root mean square error of $6.95\ \mu mol\ m^{-2}\ s^{-1}$ (see Kumagai et al., 2006).

Fig. 4 illustrates the measured diurnal patterns of N_E, by combining all data from 1 June 2001 to 29 October 2002 and plotting the diurnal values within the first and third quartiles, which reduces the influence of outliers. On wet days with a rainfall event during the daylight hours (Fig. 4a-1), there were apparent N_E declines of around 1.0–1.5 $\mu mol\ m^{-2}\ s^{-1}$ between 1000 and 1500 LT observed, as compared to wet days without daytime rainfall (Fig. 4a-2), because of the frequent occurrence of rainfall events (see Fig. 1B and C). Measured values of N_E on wet days without daytime rainfall were slightly less than those on dry days (see Fig. 4a-2 and b). This implies that there might be cloud cover effects during daytime, even on wet days without daytime rainfall. On all wet days (284 days) (Fig. 4a), the N_E between 1200 and 1500 LT was apparently reduced; however, the average diurnal values during that period were not significantly reduced. On the other hand, there was an appreciably wide range of measured N_E during all daylight hours on dry days (213 days) (Fig. 4b) despite there being no rainfall owing to the constant presence of clouds over this tropical rainforest region (Kumagai et al., 2001). As a result, there was little significant difference in the average diurnal pattern of measured N_E between wet and dry day conditions. Thus, the diurnal values on wet days little affected the values on a whole-year scale in terms of both their range and average (Fig. 4c).

Table 1
Mean model-estimated N_E (±standard deviation) from 1000 ± 1400 LT for each condition – wet days with and without daytime rainfall, all wet days, dry days, and the full year.

Condition	N_E ($\mu mol\ m^{-2}\ s^{-1}$)
Wet days with daytime rainfall	$-17.3^{a} \pm 7.2$
Wet days without daytime rainfall	$-18.3^{bc} \pm 6.4$
All wet days	$-17.4^{a} \pm 7.1$
Dry days	$-18.7^{b} \pm 5.1$
Full year	$-17.9^{ac} \pm 6.1$

Superscripts denote differences in condition, from the Cochran–Cox test ($P < 0.05$).

N_E values for wet days with and without daytime rainfall, all wet days, dry days, and the entire year were computed using time series of meteorological factors generated by a 1000-day run for each of the wet- and dry-day conditions (also shown in Fig. 4). The model estimated N_E averaged over 1000–1400 LT (the period when N_E peaked) for each condition was represented with the standard deviation and statistical significance of differences between the means in Table 1. The value for wet days with daytime rainfall does not significantly differ from that for all wet days, and thus, mainly contributes to that for all wet days. The modeled mean diurnal patterns of N_E agreed well with medians of the measurements for wet days and the whole year, but were slightly overestimated for dry days. In addition, it should be noted that the modeled N_E averaged over 1000–1400 LT on wet days (Fig. 4a) can be up to 93% of that on dry days (Fig. 4b) despite the wet days having a rainfall peak around 1300–1400 LT (see Fig. 1B and C), and that the diurnal pattern of N_E for the whole year (Fig. 4c) was little affected by that for the wet days (Table 1). Thus, we inferred from the small overestimation the validities of the observed similarity in diurnal N_E between wet and dry days and the small influence of the wet-day N_E on the mean diurnal pattern of N_E on a whole-year scale in LHNP. There are always clouds over the study region, which causes the wide day-to-day and within-day variations in the diurnal N_E pattern. However, in reality, the mean R_s (±the standard deviation) at 1000–1400 LT was significantly larger for dry days ($673.4 \pm 190.2\ W\ m^{-2}$) than for wet days ($554.7 \pm 245.2\ W\ m^{-2}$). Thus, the similar N_E values for wet and dry days might be attributed to the light saturation of N_E at relatively low incident radiative energy in this forest ecosystem rather than the cloud effect under the dry-day condition, which is examined in the following.

Fig. 5 shows frequency distributions of R_s and vapor pressure deficit (D; kPa) at 1200–1400 LT, when there was the highest probability of rainfall during a day, for (i) rainfall events, (ii) no rainfall on wet days, and (iii) dry days. Here, case (ii) relates mostly to rainfall events at night. Frequencies of high R_s and D varied greatest in the order (i) < (ii) < (iii), and the mean values of R_s and D were $218.8\ W\ m^{-2}$ and 0.22 kPa, respectively, for (i), $574.4\ W\ m^{-2}$ and 0.84 kPa for (ii), and $669.7\ W\ m^{-2}$ and 1.24 kPa for (iii). Lower values for (ii) than for (iii) might reflect a cloud-cover effect. SVAT-modeled N_E, despite being a function of many environmental factors, were plotted against R_s in Fig. 6a, and could be well fitted to a function of R_s and D ($R^2 = 0.85$). It should be noted that this modeled light response curve captured the canonical form of the measurements despite having a tendency of overestimation (Fig. 6a). While N_E was low at low light intensity occurring mainly during rainfall events, it became saturated at around $500\ W\ m^{-2}$, resulting in similar N_E values for (ii) and (iii) (Figs. 5a and 6a). The

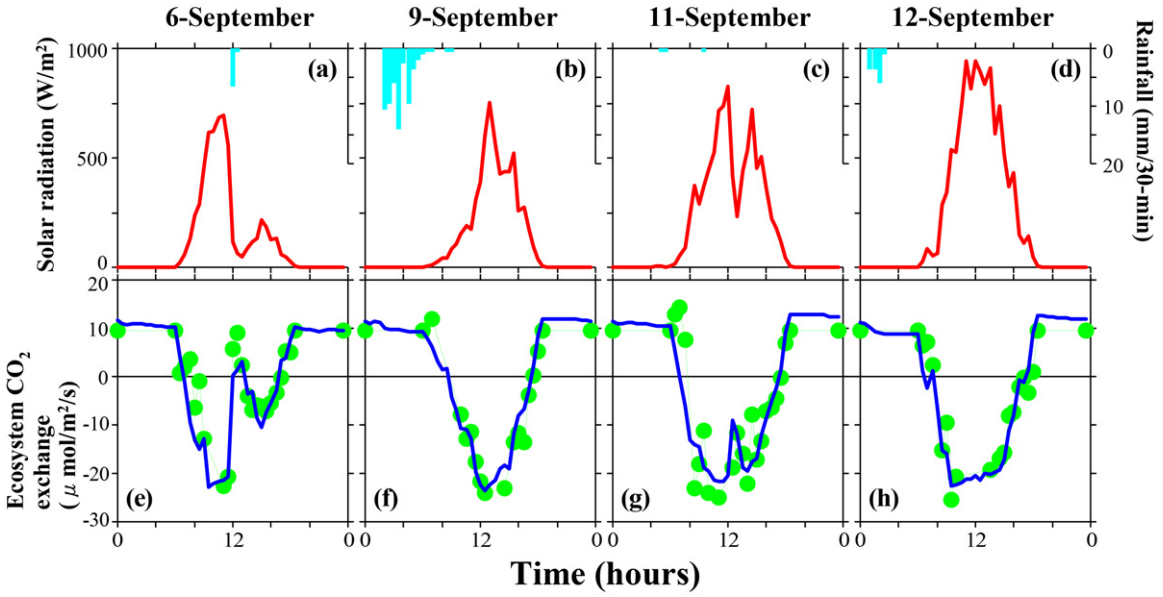

Fig. 3. Diurnal patterns of rainfall (bars) and solar radiation (lines) (a–d), and measured (closed circles) and modeled (lines) ecosystem CO_2 exchange (e–h) in LHNP from 6 to 12 September 2002.

ratio of diffuse radiation to total R_s at around 1200–1400 LT linearly decreases with the R_s increasing, resulting in a peak value of diffuse radiation (approximately 350 W m^{-2}) at $R_s \approx 540$ W m^{-2} (see Kumagai et al., 2006). This implies that R_s is absorbed by canopies efficiently up to around 500 W m^{-2}, and the canopy assimilation thus becomes saturated at that value. We then quantified the variability in N_E with changes in states R_s and D, using the chain rule ($\Delta N_E = (\partial N_E/\partial R_s)\Delta R_s + (\partial N_E/\partial D)\Delta D$) (Fig. 6b). The contribution of variation in D to the total N_E change ($(\partial N_E/\partial D)\Delta D$) revealed that D little affected N_E in this ecosystem. Here, it is interesting to note that based on a prior study, the primary forcing variable for transpiration at the study site is net available energy (Kumagai et al., 2005). Again, we have to note that the frequency of low R_s during 1200–1400 LT, which mostly occurred during rainfall events, was very small in the total frequency distribution of R_s (Fig. 5a). In summary, rainfall events significantly reduced N_E through the low-light-intensity effect, but did not affect annual-scale N_E because of the short rainfall duration. It should be noted that the rainfall duration in LHNP is exceptionally short (<3% of total hours in a day) compared with that of other tropical rainforests (Kume et al., 2011). Additionally, the light saturation of N_E at a relatively low incident radiative energy (≈500 W m^{-2} of solar radiation) is attributed to the similar N_E values for wet and dry days despite their different light environments because of cloud cover.

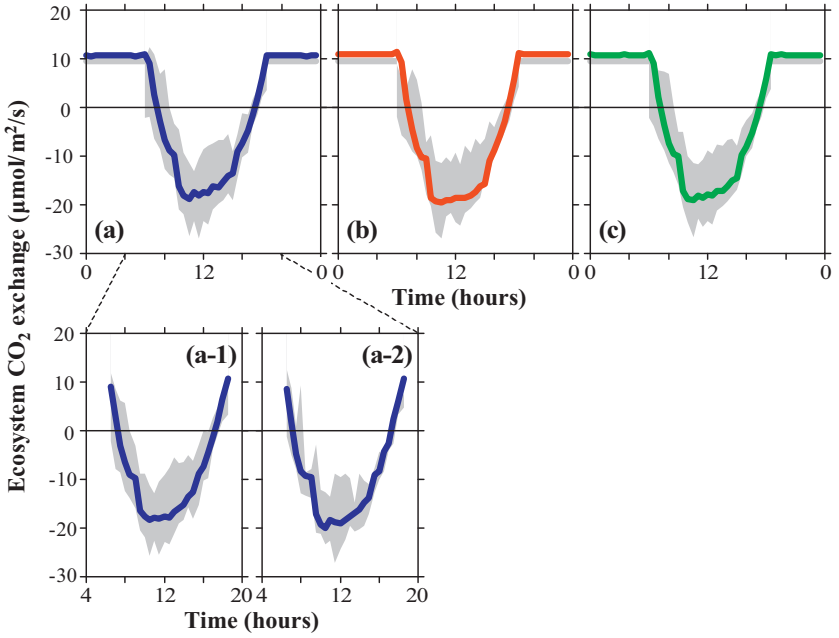

Fig. 4. Temporal variations in measured (gray zones) and average modeled (lines) ecosystem CO_2 exchange for wet days (a), dry days (b) and the whole year (c) in LHNP. Wet and dry days refer to those with and without rainfall events during the entire day, respectively, and (a-1) and (a-2) are for wet days with and without rainfall events during daylight hours, respectively. Lower and upper boundaries of the gray zone denote first and third quartiles of observations in the period 1 June 2001–29 October 2002, respectively. Measurement data were for 284 wet days and 213 dry days.

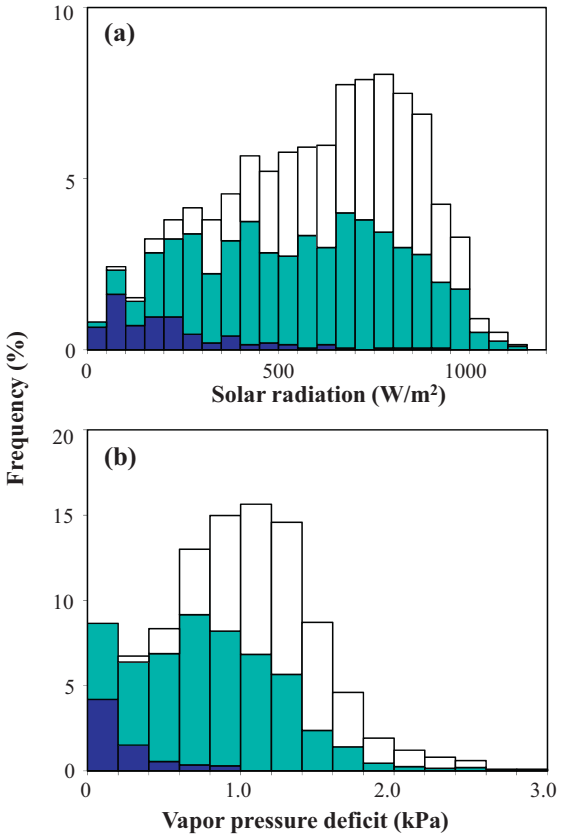

Fig. 5. Frequency distribution of solar radiation (a) and vapor pressure deficit (b) at 1200–1400 LT in LHNP. Light shading, dark shading, and no shading denote wet days without rainfall during 1200–1400 LT, rainfall events, and dry days, respectively. Wet and dry days refer to those with and without rainfall events during the entire day, respectively.

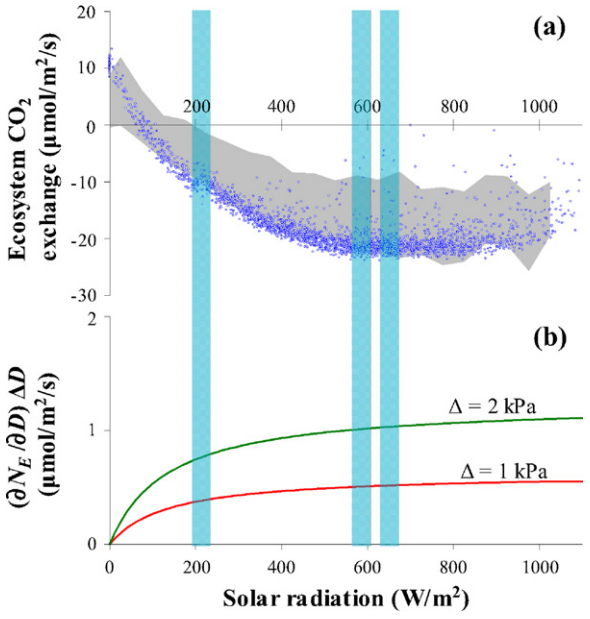

Fig. 6. SVAT-modeled (circles) and measured (gray zone) ecosystem CO_2 exchange (N_E) (a) and contribution of variation in vapor pressure deficit (D) to total N_E change ($(\partial N_E/\partial D)\Delta D$), (b) as functions of solar radiation (R_s). Lower and upper boundaries of the gray zone denote first and third quartiles of observations in the period 1 June 2001–29 October 2002, respectively. Shaded columns denote zones around mean R_s values for dry days, wet days without rainfall, and rainfall events (see Fig. 4).

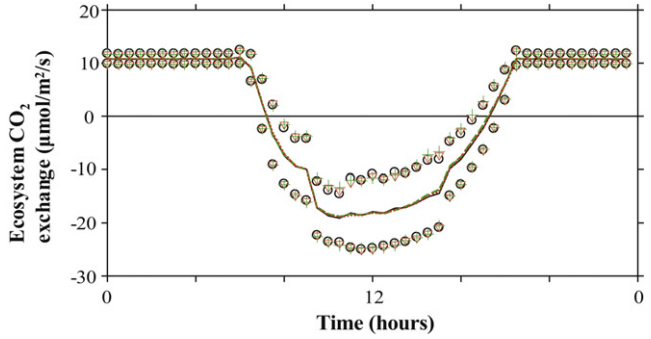

Fig. 7. Average diel variations in modeled ecosystem CO_2 exchange for the whole year with ±1 standard deviations (SD) in LHNP (solid line with circles), Bintulu (dotted line with triangles) and Kuching (broken line with crosses). Upper and lower symbols denote plus and minus one SD, respectively. Note that all three lines almost perfectly overlap.

4.2. Analyses for Bintulu and Kuching

To understand the meaning of the diurnal precipitation cycle for N_E in this tropical rainforest region, further numerical experiments were conducted assuming that the LHNP rainforest ecosystem was located in Bintulu and Kuching, which have different diurnal rainfall cycle characteristics from that in LHNP (see Fig. 1A), and the results are shown in Fig. 7. Note that for these computations, we replaced only rainfall temporal patterns (including rainfall amount) of LHNP with those of Bintulu and Kuching and kept the relationships between rainfall intensity and other environmental factors such as R_s the same as for LHNP. The strongest rainfall peak in the diurnal rainfall cycle in LHNP resulted in the lowest N_E at around 1300–1400 LT at the three sites, but the difference was very slight (data not shown here). Additionally, there were differences in the variability of N_E among the three sites (e.g., at 1030 and 1500 LT) but these were very slight (Fig. 7). As a result, there was no or little difference in the whole-year N_E among these three sites (Fig. 7). This confirms that the diurnal rainfall cycle does not significantly affect the diurnal cycle of incident radiative energy in the studied tropical rainforest region because the contribution of rainfall duration to total time is still small, and that the productivity of the tropical rainforest ecosystem might be somewhat conservative in terms of its similarity over the tropical rainforest region. This is because of the combined effects of the light response of N_E being saturated at relatively low light intensity and the constant cloud cover.

5. Conclusion

There was little difference in the mean diurnal N_E pattern between wet and dry days, and the diurnal rainfall regime little affected N_E on a whole-year scale. Similar N_E values for wet and dry days were attributed to a minor contribution of lower N_E during rainfall events to total N_E in wet conditions. This was because of constant cloud cover on both wet and dry days, and the light saturation of N_E at relatively low incident radiative energy in this forest ecosystem. Regarding cloud cover effects in tropical forests, cloud forests where there is constant cloudiness, and seasonal forests in the dry season where there is mostly clear sky, could be the end members. The analyses here would be a promising tool for assessing those forest ecosystem productivities and, in turn, application of the analyses to those types of forests would sufficiently validate the SVAT model of this study.

The effect of rainfall on N_E is due to not only the effects of R_s and D, but also the change in soil moisture with rainwater supply, which affects stomatal behavior and soil respiration. However, in this study, we assumed that there is little risk of a shortage of ecosystem

water resources in the studied region (see Kumagai and Porporato, 2012) and little soil moisture effect on N_E. The slight dependency of soil respiration on soil moisture has been detected in LHNP (Ohashi et al., 2008), but soil moisture depletion leading to reduced soil respiration was believed to seldom occur in the study region. Also, previous studies have suggested that evapotranspiration is a conservative process in terms of its similarity for pan-tropical forests, because net radiation is the strongest determinant and can explain seasonal and spatial variations in forest water use (e.g., Kumagai et al., 2005; Fisher et al., 2009), and this can be partly explained by little risk of water-stress-induced hydraulic failure of plants (see Kumagai and Porporato, 2012). This implies that given the similar incident radiative energy among forest ecosystem sites, the water vapor fluxes accompanied by stomatal conductance and assimilation are also similar among the sites, which might support the findings of how forest canopy and/or meteorological characteristics caused the similar N_E among the three studied sites.

Acknowledgments

We are grateful to the Forestry Department, Sarawak, for their support during this study. We also thank Tohru Nakashizuka, Masakazu Suzuki and Tetsukazu Yahara for their support and numerous colleagues who helped us with this work. This work was funded by Core Research for Evolutional Science and Technology (CREST) of the Japan Science and Technology Agency (JST), the Global COE (Centers of Excellence) Program (GCOE) of the Japan Society for the Promotion of Science (JSPS), grants from the Ministry of Education, Science and Culture, Japan (#20248016, #21255001, #23255002, and #23405028).

References

Badger, M.R., Collatz, G.J., 1977. Studies on the Kinetic Mechanism of Ribulose-1,5-Bisphosphate Carboxlase and Oxygenase Reactions, with Particular Reference to the Effect of Temperature on Kinetic Parameters. Carnegie Institute of Washington Yearbook, Washington, pp. 355–361.

Ball, J.T., Woodrow, I.E., Berry, J.A., 1987. A model predicting stomatal conductance and its contribution to the control of photosynthesis under different environmental conditions. In: Biggens, J. (Ed.), Progress in Photosynthesis Research. Springer, New York, pp. 221–224.

Campbell, G.S., Norman, J.M., 1998. An Introduction to Environmental Biophysics, 2nd ed. Springer, New York.

Collatz, G.J., Ball, J.T., Grivet, C., Berry, J.A., 1991. Physiological and environmental regulation of stomatal conductance, photosynthesis and transpiration: a model that includes a laminar boundary layer. Agricultural and Forest Meteorology 54, 107–136.

Daly, E., Oishi, A.C., Porporato, A., Katul, G.G., 2008. A stochastic model for daily subsurface CO_2 concentration and related soil respiration. Advances in Water Resources 31, 987–994.

de Pury, D.G.G., Farquhar, G.D., 1997. Simple scaling of photosynthesis from leaves to canopies without the errors of big-leaf models. Plant, Cell & Environment 20, 537–557.

Farquhar, G.D., von Caemmerer, S., Berry, J.A., 1980. A biochemical model of photosynthetic CO_2 assimilation in leaves of C_3 species. Planta 149, 78–90.

Farquhar, G.D., Wong, S.C., 1984. An empirical model of stomatal conductance. Australian Journal of Plant Physiology 11, 191–210.

Fisher, J.B., Malhi, Y., Bonal, D., da Rocha, H.R., de Araujo, A.C., Gamo, M., Goulden, M.L., Hirano, T., Huete, A.R., Kondo, H., Kumagai, T., Loescher, H., Miller, S., Nobre, A.D., Nouvellon, Y., Oberbauer, S., Panuthai, S., Roupsard, O., Saleska, S., Tanaka, K., Tanaka, N., Tu, K.P., von Randow, C., 2009. The land-atmosphere water flux in the tropics. Global Change Biology 15, 2694–2714.

Goudriaan, J., 1977. Crop Micrometeorology: A Simulation Study. Centre for Agricultural Publishing, Documentation, Wageningen.

Huxman, T.E., Snyder, K.A., Tissue, D., Leffler, A.J., Ogle, K., Pockman, W.T., Sandquist, D.R., Potts, D.L., Schwinning, S., 2004. Precipitation pulses and carbon fluxes in semiarid and arid ecosystems. Oecologia 141, 254–268.

Ichikawa, H., Yasunari, T., 2006. Time-space characteristics of diurnal rainfall over Borneo and surrounding oceans as observed by TRMM-PR. Journal of Climatology 19, 1238–1260.

Katul, G.G., Albertson, J.D., 1998. An investigation of higher-order closure models for a forested canopy. Boundary Layer Meteorology 89, 47–74.

Katul, G.G., Albertson, J.D., 1999. Modeling CO_2 sources, sinks, and fluxes within a forest canopy. Journal of Geophysical Research 104, 6081–6091.

Knapp, A.K., Fay, P.A., Blair, J.M., Collins, S.L., Smith, M.D., Carlisle, J.D., Harper, C.W., Danner, B.T., Lett, M.S., McCarron, J.K., 2002. Rainfall variability, carbon cycling, and plant species diversity in a mesic grassland. Science 298, 2202–2205.

Kumagai, T., Ichie, T., Yoshimura, M., Yamashita, M., Kenzo, T., Saitoh, T.M., Ohashi, M., Suzuki, M., Koike, T., Komatsu, H., 2006. Modeling CO_2 exchange over a Bornean tropical rain forest using measured vertical and horizontal variations in leaf-level physiological parameters and leaf area densities. Journal of Geophysical Research 111, D10107, http://dx.doi.org/10.1029/2005JD006676.

Kumagai, T., Katul, G.G., Porporato, A., Saitoh, T.M., Ohashi, M., Ichie, T., Suzuki, M., 2004a. Carbon and water cycling in a Bornean tropical rainforest under current and future climate scenarios. Advances in Water Resources 27, 1135–1150.

Kumagai, T., Kuraji, K., Noguchi, H., Tanaka, Y., Tanaka, K., Suzuki, M., 2001. Vertical profiles of environmental factors within tropical rainforest, Lambir Hills National Park, Sarawak Malaysia. Journal of Forest Research 6, 257–264.

Kumagai, T., Porporato, A., 2012. Strategies of a Bornean tropical rainforest water use as a function of rainfall regime: isohydric or anisohydric? Plant, Cell & Environment 35, 61–71.

Kumagai, T., Saitoh, T.M., Sato, Y., Morooka, T., Manfroi, O.J., Kuraji, K., Suzuki, M., 2004b. Transpiration, canopy conductance and the decoupling coefficient of a lowland mixed dipterocarp forest in Sarawak, Borneo: dry spell effects. Journal of Hydrology 287, 237–251.

Kumagai, T., Saitoh, T.M., Sato, Y., Takahashi, H., Manfroi, O.J., Morooka, T., Kuraji, K., Suzuki, M., Yasunari, T., Komatsu, H., 2005. Annual water balance and seasonality of evapotranspiration in a Bornean tropical rainforest. Agricultural and Forest Meteorology 128, 81–92.

Kumagai, T., Yoshifuji, N., Tanaka, N., Suzuki, M., Kume, T., 2009. Comparison of soil moisture dynamics between a tropical rainforest and a tropical seasonal forest in Southeast Asia: impact of seasonal and year-to-year variations in rainfall. Water Resources Research 45, W04413, http://dx.doi.org/10.1029/2008-WR007307.

Kume, T., Kuraji, K., Yoshifuji, N., Morooka, T., Sawano, S., Chong, L., Suzuki, M., 2006. Estimation of canopy drying time after rainfall using sap flow measurements in an emergent tree in a lowland mixed-dipterocarp forest in Sarawak Malaysia. Hydrological Processes 20, 565–578.

Kume, T., Tanaka, N., Kuraji, K., Komatsu, H., Yoshifuji, N., Saitoh, T.M., Suzuki, M., Kumagai, T., 2011. Ten-year evapotranspiration estimates in a Bornean tropical rainforest. Agricultural and Forest Meteorology 151, 1183–1192.

Mabuchi, K., Sato, Y., Kida, H., 2005. Climatic impact of vegetation change in the Asian tropical region: Part I. Case of the Northern Hemisphere summer. Journal of Climate 18, 410–428.

Malhi, Y., Wright, J., 2004. Spatial patterns and recent trends in the climate of tropical rainforest regions. Philosophical Transactions of the Royal Society of London Series B 359, 311–329.

Manfroi, O.J., Kuraji, K., Suzuki, M., Tanaka, N., Kume, T., Nakagawa, M., Kumagai, T., Nakashizuka, T., 2006. Comparison of conventionally observed interception evaporation in a 100-m^2 subplot with that estimated in a 4-ha area of the same Bornean lowland tropical forest. Journal of Hydrology 329, 329–349.

Mellor, G.L., 1973. Analytic prediction of the properties of stratified planetary surface layers. Journal of the Atmospheric Sciences 30, 1061–1069.

Nesbitt, S.W., Zipser, E.J., 2003. The diurnal cycle of rainfall and convective intensity according to three years of TRMM measurements. Journal of Climate 16, 1456–1475.

Nobre, C.A., Sellers, P.J., Shukla, J., 1991. Amazonian deforestation and regional climate change. Journal of Climate 4, 957–988.

Ohashi, M., Kumagai, T., Kume, T., Gyokusen, K., Saitoh, T.M., Suzuki, M., 2008. Characteristics of soil CO_2 efflux variability in an aseasonal tropical rainforest in Borneo Island. Biogeochemistry 90, 275–289.

Ohsawa, T., Hayashi, T., Mitsuta, Y., Matsumoto, J., 2001. Dirunal variations of convective activity and rainfall in tropical Asia. Journal of the Meteorological Society of Japan 79, 333–352.

Oki, T., Musiake, K., 1994. Seasonal change of the diurnal cycle of precipitation over Japan and Malaysia. Journal of Applied Meteorology 33, 1445–1463.

Palmroth, S., Maier, C.A., McCarthy, H.R., Oishi, A.C., Kim, H.-S., Johnsen, K.H., Katul, G.G., Oren, R., 2005. Contrasting responses to drought of forest floor CO_2 efflux in a Loblolly pine plantation and a nearby Oak-Hickory forest. Global Change Biology 11, 1–14.

Tanaka, K., 2002. Multi-layer model of CO_2 exchange in a plant community coupled with the water budget of leaf surfaces. Ecological Modelling 147, 85–104.

Taylor, H.M., Karlin, S., 1998. An Introduction to Stochastic Modeling, 3rd ed. Academic Press, San Diego.

Taylor, J.A., Lloyd, J., 1992. Sources and sinks of atmospheric CO_2. Australian Journal of Biotechnology 40, 407–418.

Timmermann, A., Oberhuber, J., Bacher, A., Esch, M., Latif, M., Roeckner, E., 1999. Increased El Niño frequency in a climate model forced by future greenhouse warming. Nature 398, 694–697.

von Caemmerer, S., Evans, J.R., Hudson, G.S., Andrews, T.J., 1994. The kinetics of ribulose-1,5-bisphosphate carboxylase/oxygenase in vivo inferred from measurements of photosynthesis in leaves of transgenic tobacco. Planta 195, 88–97.

von Caemmerer, S., Farquhar, G.D., 1981. Some relationships between the biochemistry of photosynthesis and the gas exchange of leaves. Planta 153, 376–387.

Watanabe, T., 1993. The bulk transfer coefficients over a vegetated surface based on K-theory and a 2nd-order closure model. Journal of the Meteorological Society of Japan 71, 33–42.

Werth, D., Avissar, R., 2005. The local and global effects of Southeast Asian deforestation. Geophysical Research Letters 32, L20702, http://dx.doi.org/10.1029/2005GL022970.

Wilson, N.R., Shaw, R.H., 1977. A higher order closure model for canopy flow. Journal of Applied Meteorology 16, 1197–1205.